COMPRESSION OF A TUMBLING VORTEX: A LES AND PANS STUDY

S. Jakirlic, C.-Y. Chang and C. Tropea
Institute of Fluid Mechanics and Aerodynamics / Center of Smart Interfaces
Technische Universität Darmstadt
Petersenstr. 30 / 32, D-64287 Darmstadt, Germany
s.jakirlic@sla.tu-darmstadt.de, chang@sla.tu-darmstadt.de, ctropea@sla.tu-darmstadt.de

B. Basara
Advanced Simulation Technology, AVL List GmbH
Hans-List-Platz 1, A-8020 Graz, Austria
branislav.basara@avl.com

ABSTRACT

In this paper we report on parallel LES (Large Eddy Simulation) and PANS (Partial-Averaged Navier-Stokes) study of the flow and turbulence in the process of the tumbling vortex generation and their response to the consequently imposed compression. Reference database was provided by Borée et al. (2002) who designed a square-piston compression machine to investigate experimentally the generation and breakdown of a tumbling motion. The computational approach whose validation represents the main objective of the present work is the so-called PANS method, proposed recently by Girimaji (2006), which provides a seamless transition from Unsteady RANS to the direct numerical solution (DNS) as the unresolved-to-total ratios of kinetic energy and its dissipation are varied.

Whereas the results obtained by both methods exhibit reasonable agreement of the mean velocity field with reference database during both the intake and compression strokes, the predicted turbulence enhancement during the compression stroke is somewhat retarded.

INTRODUCTION

The internal aerodynamics of reciprocating engines has a strong influence on the engine combustion process, and consequently, on the engine efficiency and emission of pollutants. The flow in piston-cylinder assemblies relevant to an IC engine is strongly influenced by joint action of different phenomena such as injecting jets, tumbling and swirling motion, wall shear and confinement, expansion and compression. Accordingly, a complex unsteady recirculating flow pattern and cyclic large-scale motion is generated. Furthermore the flow is featured by strong and highly anisotropic turbulence. Design and optimisation of internal combustion engines is nowadays intensively supported by the Computational Fluid Dynamics packages. The common practice in predicting engine flow is to use the Reynolds-averaged Navier-Stokes (RANS) models. However, the RANS models are single point closures relying on the assumption of self-similarity of the turbulence spectrum, the fact leading to only one characteristic turbulence length scale, defining the entire spectrum. Consequently, the physics of the flows dominated by the organized, large-scale coherent structures could not be captured satisfactorily in such a way. Therefore, an LES-related (Large-Eddy Simulation), eddy-resolving scheme should be employed in order to correctly capture flow phenomena mentioned above. It is in accordance with the conclusions drawn by Rutland (2011) in his review of the LES feasibility of computing the internal-combustion engine flows.

The work reported here aims at validation of a seamless hybrid LES/RANS method denoted as PANS in conjunction with the universal wall treatment, in such a complex flow configuration. The PANS method should capture the unsteady flow features more accurately compared to the conventional URANS (Unsteady RANS) method.

FLOW CONFIGURATION DESCRIPTION

Borée et al. (2002) designed a square-cylinder (with the cross-section $b \times b = 100 \times 100\ mm^2$) compression machine equipped with a flat head piston (Fig. 1) to investigate the generation and breakdown of a tumbling motion experimentally (a relevant computational study using LES method was performed by Toledo et al., 2007). This simple geometry, in comparison with a realistic Internal Combustion (IC) engine, provides well defined boundary conditions and good optical access. Detailed PIV (Particle Image Velocimetry) data corresponding to the evolution of the vortex induced during the intake process and its consequent compression were generated. The data set comprises fluctuating and phase-averaged (over 120 cycles) velocity and turbulence fields measured in the central plane of the compression chamber. Kinematics of the piston movement is described by a sinusoidal function, Toledo et al. (2007): $a(t) = b - (V_p / \omega)(1 + \cos(\omega t))$, with ωt representing the crank angle (CA) and the maximum piston velocity $V_p = 0.809\ m/s$. The length of the square cylinder volume at the Top-Dead-Center (TDC) – pertinent to the compression stroke - corresponds to $a_{min} = 25\ mm$. The piston stroke – the way the piston has to cover until reaching the Bottom-Dead-Center (BDC) at the end of the intake stroke, i.e. at the beginning of the compression stroke – amounts *75 mm*. Accordingly, the compression ratio (CR), representing the ratio of the maximum chamber volume ($b^2 a_{max}$; with $a_{max} = 100\ mm$) to the current one, takes the values between 4 (TDC) and 1 (BDC). The inflow system

represents a channel functioning as an "intake/outtake valve" in a four-stroke engine, being opened during the intake stroke (every uneven expansion) and the exhaust stroke (every even compression) and closed in all remaining expansion and compression cycles, see e.g. Fig. 2. The dimensions of this eccentrically positioned channel (see Fig. 1) are (*length*, *height*, *width*)=(*300 mm*, *10 mm*, *96 mm*). The channel flow Reynolds number during the intake stroke corresponds approximately to 12000. It is assumed, according to the *length/height* ratio – *300/10=30*, that the near-wall flow at the inlet of the compression chamber corresponds to the fully-developed turbulence.

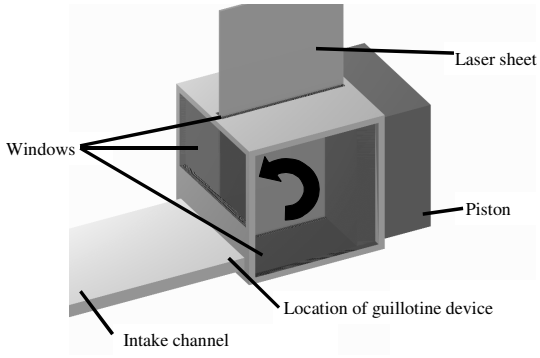

Figure 1: Schematic of the compression chamber (adopted from Borée et al., 2002)

COMPUTATIONAL MODEL

The three-dimensional, incompressible unsteady continuity and momentum equations governing the velocity field in the compression chamber read

$$\frac{\partial \rho}{\partial t} + \rho \frac{\partial \left(\overline{U}_j - U_{bj} \right)}{\partial x_j} = 0 \qquad (1)$$

$$\frac{\partial \left(\rho \overline{U}_i \right)}{\partial t} + \rho \frac{\partial \left[\overline{U}_i \left(\overline{U}_j - U_{bj} \right) \right]}{\partial x_j} = -\frac{\partial \overline{p}}{\partial x_i} + \frac{\partial}{\partial x_j} \left(\overline{\tau}_{ij}^{\mu} + \overline{\tau}_{ij}^{t} \right) \qquad (2)$$

where U_{bi} stands for the velocities of moving boundaries of the computational domain. In the case of the present 1-D compression $U_{bi} = (V_p, 0, 0)$ with V_p representing the piston velocity. The velocity U_{bi} is to be determined by solving an additional equation describing conservation of space – in accordance to the space conservation law, see e.g. Demirdzic and Peric, 1990 - simultaneously with the continuity and momentum equations. By assuming that acoustic waves have an insignificant effect on the turbulence (e.g., Reynolds, 1980), the fluctuating field can be viewed as being incompressible (divergence free), interacting with a compressed mean flow. Accordingly, the mean gas density changes are approximated as being only a function of time and temperature. The time variation of viscosity is accounted for by a power-law (see e.g., White, 1974) under the condition of an adiabatic process. In Eq. (2)

$$\overline{\tau}_{ij}^{\mu} = 2\mu \overline{S}_{ij} - \frac{2}{3} \mu \overline{S}_{kk} \delta_{ij}; \quad \overline{S}_{ij} = \frac{1}{2} \left(\frac{\partial \overline{U}_i}{\partial x_j} + \frac{\partial \overline{U}_j}{\partial x_i} \right)$$

represents the viscous stress tensor. The turbulent stress tensor representing either subgrid-stress tensor in the LES framework or the Reynolds stress tensor (mimicking the subgrid-scale stress tensor) in the PANS-framework is expressed in terms of the mean strain tensor via the Boussinesq relationship:

$$\overline{\tau}_{ij}^{t} \equiv -\rho \overline{\tau}_{ij} = \mu_{SGS} \left(\frac{\partial \overline{U}_i}{\partial x_j} + \frac{\partial \overline{U}_j}{\partial x_i} - \frac{2}{3} \frac{\partial \overline{U}_k}{\partial x_k} \delta_{ij} \right) - \frac{2}{3} \rho \delta_{ij} \overline{\tau}_{kk} \qquad (3)$$

$$\overline{\tau}_{ij}^{t} \equiv -\rho \overline{u_i u_j} = \mu_t \left(\frac{\partial \overline{U}_i}{\partial x_j} + \frac{\partial \overline{U}_j}{\partial x_i} - \frac{2}{3} \frac{\partial \overline{U}_k}{\partial x_k} \delta_{ij} \right) - \frac{2}{3} \rho k \delta_{ij} \qquad (4)$$

For the determination of the turbulent viscosity within the LES framework the most widely used subgrid-scale model of Smagorinsky, representing a zero-equation model, is adopted with the eddy-viscosity of the residual motion:

$$\mu_{SGS} = \rho \left(C_S \Delta \right)^2 \left| \overline{S} \right|; \Delta = \left(\Delta_x \Delta_y \Delta_z \right)^{1/3}; \left| \overline{S} \right| = \left(2 \overline{S}_{ij} \overline{S}_{ij} \right)^{1/2} \qquad (5)$$

modeled in terms of the representative mesh size (filter width) Δ and the strain rate modulus; the Smagorinsky constant C_S takes the value of 0.1.

PANS. The Partially-Averaged Navier-Stokes (PANS) approach proposed recently by Girimaji (2006), enables seamlessly a smooth transition from RANS to the direct numerical solution of the Navier-Stokes equations (DNS) as the unresolved-to-total ratios of kinetic energy ($f_k=k_u/k$) and dissipation ($f\varepsilon=\varepsilon_u/\varepsilon$) are varied. The equations governing the unresolved kinetic energy k_u and corresponding unresolved dissipation rate ε_u are systematically derived from the standard k-ε model:

$$\frac{Dk_u}{Dt} = \left(P_u - \varepsilon_u \right) + \frac{\partial}{\partial x_j} \left[\left(\nu + \frac{\nu_u}{\sigma_{ku}} \right) \frac{\partial k_u}{\partial x_j} \right] \qquad (6)$$

$$\frac{D\varepsilon_u}{Dt} = C_{\varepsilon 1} P_u \frac{\varepsilon_u}{k_u} - C_{\varepsilon 2}^{*} \frac{\varepsilon_u^2}{k_u} + \frac{\partial}{\partial x_j} \left[\left(\nu + \frac{\nu_u}{\sigma_{\varepsilon u}} \right) \frac{\partial \varepsilon_u}{\partial x_j} \right] \qquad (7)$$

Here, the eddy viscosity of the unresolved scales takes its standard form $\nu_u = C_\mu k_u^2 / \varepsilon_u$. The form of the functional dependency in the model coefficients is of decisive importance. This is especially the case with the coefficient multiplying the destruction term in the dissipation equation. The appropriate formulation is given by

$$C_{\varepsilon 2}^{*} = C_{\varepsilon 1} + \frac{f_k}{f_\varepsilon} \left(C_{\varepsilon 2} - C_{\varepsilon 1} \right); \quad \sigma_{k,\varepsilon u} = \sigma_{k,\varepsilon} \frac{f_k^2}{f_\varepsilon} \qquad (8)$$

Such a model coefficient form provides a dissipation rate level which suppresses the turbulence intensity towards the subgrid (i.e. subscale) level in the region where large coherent structures with a broader spectrum dominate the flow, allowing in such a way evolution of structural features of the associated turbulence. Herewith, a seamless coupling, i.e. a smooth transition from LES to RANS and opposite is enabled. The parameter f_k is formulated in terms of the grid spacing following Basara et al. (2008)

$$f_k = \frac{1}{\sqrt{C_\mu}} \left(\frac{\Delta}{\Lambda} \right)^{2/3} \qquad (9)$$

where Δ is the grid cell size (see Eq. 5) and Λ ($= k^{3/2} / \varepsilon$) is the turbulent length scale. In this derivation the equality $\varepsilon_u = \varepsilon$ resulting in $f_\varepsilon = 1$ was assumed. The PANS asymptotic behaviour goes smoothly from RANS to DNS with decreasing f_k . In the computational procedure used here, the lowest value of the parameter f_k is adjusted to the given grid as it was implemented as a dynamic parameter, changing at each grid node. The values obtained at the end of a time step are used in the following time step.

The PANS models is applied in conjunction with the so-called universal wall treatment. This method blends the integration up to the wall (exact boundary conditions) with the wall functions, enabling well-defined boundary conditions irrespective of the position of the wall-closest computational node. This method is especially attractive for computations of industrial flows in complex domains where higher grid flexibility, i.e. weaker sensitivity against grid non-uniformities in the near wall regions, featured by different mean flow and turbulence phenomena (flow acceleration/deceleration, streamline curvature effects, separation, etc.), is desirable. Popovac and Hanjalic (2007) proposed the so-called compound wall treatment with a blending formula for the quantities specified at the central node P of the wall-closest grid cell as $\phi_P = \phi_\nu e^{-\Gamma} + \phi_t e^{-1/\Gamma}$, where 'ν' denotes the viscous and 't' the fully turbulent value. The variables ϕ apply here to the wall shear stress, production and dissipation of the turbulence kinetic energy. A somewhat simplified approach was introduced under the name "Hybrid Wall Treatment" in the numerical code AVL FIRE. Whereas the original compound wall treatment of Popovac and Hanjalic (2007) includes the tangential pressure gradient and convection, a simpler approach utilizing the standard wall functions as the "upper" bound is used presently.

Numerical method. All computations were performed using the commercial CFD software package AVL FIRE (2006). The code employs the finite volume discretization method, which rests on the integral form of the general conservation law applied to the polyhedral control volumes. All dependent variables are stored at the geometric center of the control volume. The appropriate data structure (cell-face based connectivity) and interpolation practices for gradients and cell-face values are introduced to accommodate an arbitrary number of cell faces. The convection can be approximated by a variety of differencing schemes. The diffusion is approximated using central differencing. The overall solution procedure is iterative and is based on the SIMPLE-like segregated algorithm, which ensures coupling between the velocity and pressure fields.

Computational details. The size of the solution domain (comprising the intake channel and compression chamber) corresponds closely to the experimental configuration. The channel was meshed by 241920 grid cells in total; the grid size of the compression chamber during the intake and exhaust strokes corresponds to 561600 cells (N_x, N_y, N_z=*78, 144, 50*) and during the compression and expansion strokes to 657280 cells (N_x, N_y, N_z=*52, 158, 80*). The chamber part of the solution domain accommodating the piston is deformable in accordance with the piston movement, see Fig. 4. The maximum of the non-dimensional wall distance values at the wall-next node along the chamber walls are between y^+=*0.7-0.8* (corresponding to *CA=30°* and *360°*) and *1.3-1.6* (at *CA=86°-330°*). Fig. 2. displays the field of the ratio of the characteristic grid spacing to the Kolmogorov length scale (Δ/η_K) representing one important grid quality assessment measure. This parameter takes the values well under 10.

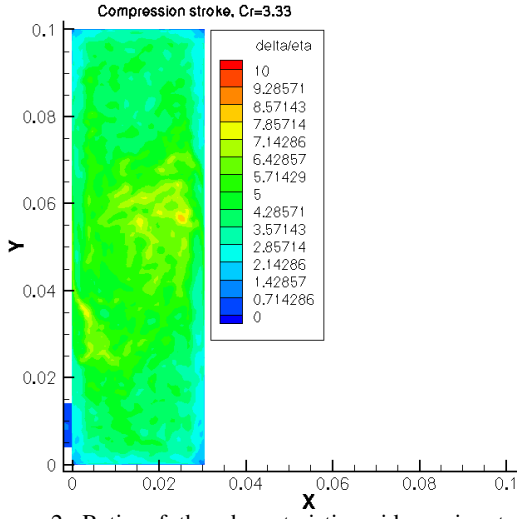

Figure 2: Ratio of the characteristic grid spacing to the Kolmogorov length scale (Δ/η_K) at *CA=330°*

The initial velocity field was generated by computing five full four-stroke cycles (atmospheric pressure was assumed at the intake channel inlet plane): intake stroke, compression stroke, expansion stroke and exhaust stroke. The phase-averaged results obtained by both LES and PANS methods correspond to ten further cycles. Fig. 3 illustrates the mean axial velocity obtained after phase-averaging of the instantaneous velocity field after ten cycles in the central vertical plane (*z=0*).

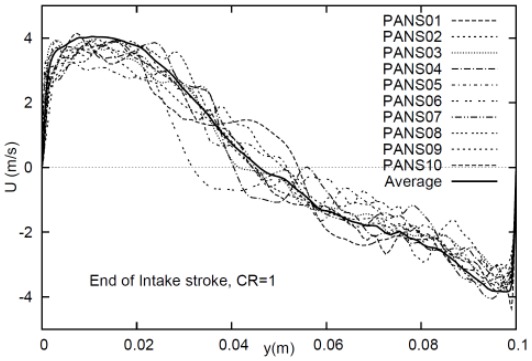

Figure 3: Profiles of the instantaneous axial velocity and their phase-averaged counterpart at CA=180°.

RESULTS AND DISCUSSION

Some selected results obtained by applying both LES and PANS at different time instants during the intake and compression strokes are depicted in Figs. 5 and 6. The

figures reveal a number of features typically associated with the highly-unsteady jet discharging from the inflow channel, separating from its sharp corners and transforming into a tumbling vortex being characterized by high velocity values. This tumbling motion occupies gradually the entire compression chamber. After onset of the compression stroke its systematic retardation takes place; the most intensive deceleration occurs along the chamber/piston walls propagating up to the vortex core; one notes the flattening of the velocity profiles in the largest portion of the cross-section. The profiles of all variables are depicted across the tumbling vortex core being characterized by the most intensive turbulence production. The maximum of the kinetic energy coincides with the position where the velocity components take zero value. It could be said in summary that both computational methods reproduced the mean flow in a reasonable agreement with the experimental results with respect to both vortex core position and velocity magnitude. This relates especially to the process of the generation of the tumbling motion. Here, the kinetic energy profiles are characterized by dual peaks, originating also from the vortex core fluctuations. This phenomenon is captured qualitatively by both simulations. Agreement weakens during the compression stroke. Velocity magnitude corresponding to the "annular" region of the tumbling vortex is somewhat underpredicted. The kinetic energy profiles reveals only one peak indicating a certain stabilization of the vortex core precession. The turbulence enhancement concentrated to the core region is qualitatively captured although with a substantial underestimation.

CONCLUSIONS

PANS and LES computations of a four-stroke rapid compression machine, for which the experimental database was provided by Borée et al. (2002), were performed. Promising results obtained by both schemes with respect to the structural characteristics of the instantaneous and phase-averaged flow field demonstrate their potential in computing such a flow configuration characterized by a broader frequency range.

REFERENCES

AVL AST, 2006. AVL Fire Manual 8.5, AVL List GmbH, Graz

Basara, B., Krajnovic, S. and Girimaji, S., 2008. PANS vs. LES for Computations of the Flow around a 3D Bluff Body. *7th Int. Symp. on Engineering Turbulence Modelling and Measurements*. Limassol, Cyprus, 4-6 June

Borée, J., Maurel, S., Bazile, R., 2002. Disruption of a compressed vortex. *Physics of Fluids*, 14(7): 2543-2556

Demirdzic, I., Peric, M., 1990. Finite volume method for prediction of fluid flow in arbitrarily shaped domains with moving boundaries. *Int. J. Numer. Meth. Fluids*, 10:771-790

Girimaji, S., 2006. Partially-Averaged Navier-Stokes Model for Turbulence: A Reynolds-Averaged Navier-Stokes to Direct Numerical Simulation Bridging Method. *J. Appl. Mech.*, 73:413-421

Popovac, M., and Hanjalic, K., 2007. Compound Wall Treatment for RANS Computation of Complex Turbulent Flows and Heat Transfer. Flow. *Turbulence and Combustion*, 78(2):177-202

Reynolds, W.C. 1980. Modelling of fluid motion in engines – an introductory overview. In: Mattavi, Amman, (Eds.), Combustion Modelling in Reciprocating Engines. Plenum Press, New York, pp. 41-68

Rutland, C.J., 2011. LES for IC engines: a review. *Int. J. of Engine Research* (to appear)

Toledo, M.S., Le Penven, L., Buffat, M., Cadiou, A. and Padilla J., 2007. Large eddy simulation of the generation and breakdown of a tumbling flow. *Int. J. heat and Fluid Flow*, 28:113-126

Acknowledgement. The financial support of the AVL List GmbH Company, Graz, Austria for C.Y. Chang is gratefully acknowledged. The authors are indebted to J. Borée (LEA, University of Poitiers) for making his experimental data available.

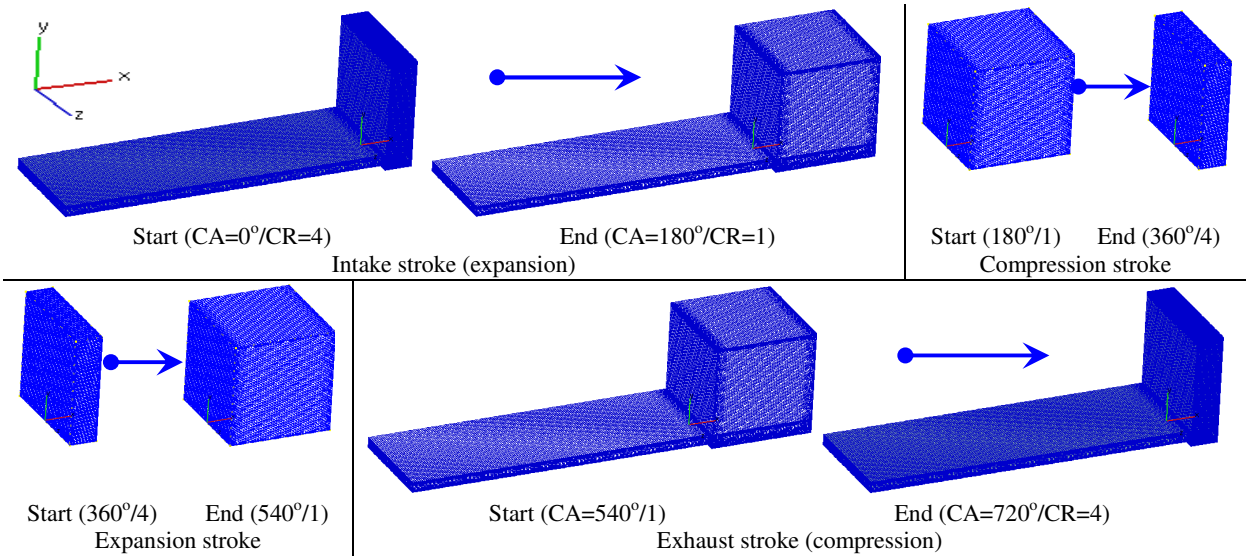

Figure 4: Temporal variation of the flow domain corresponding to different operating modes of the compression machine

CA=29.9°, CR=3.3 (intake stroke)

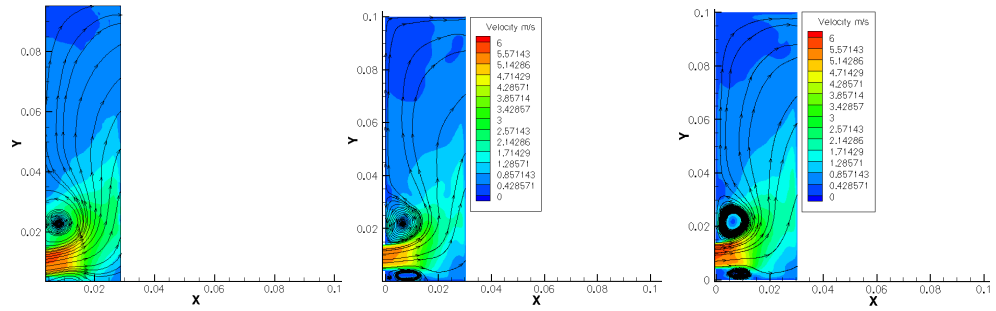

CA=86.2°, CR=1.67 (intake stroke)

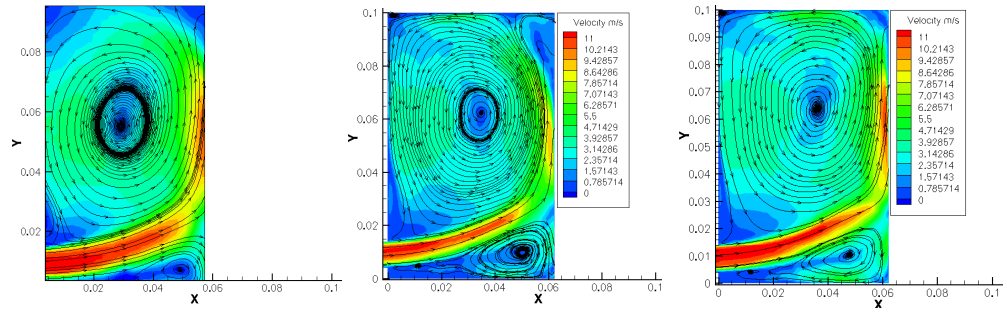

CA=180°, CR=1.0 (end of the intake stroke)

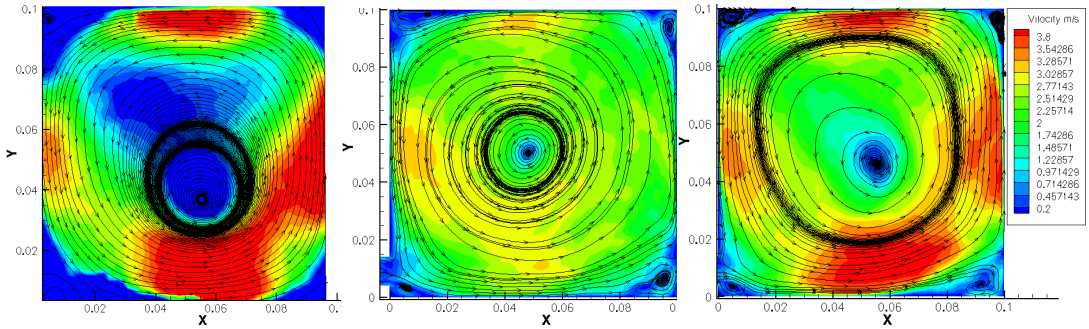

CA=273.8°, CR=1.67 (compression stroke)

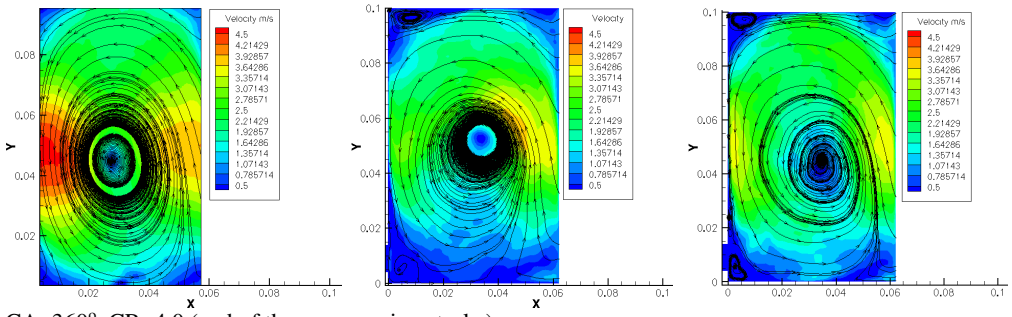

CA=360°, CR=4.0 (end of the compression stroke)

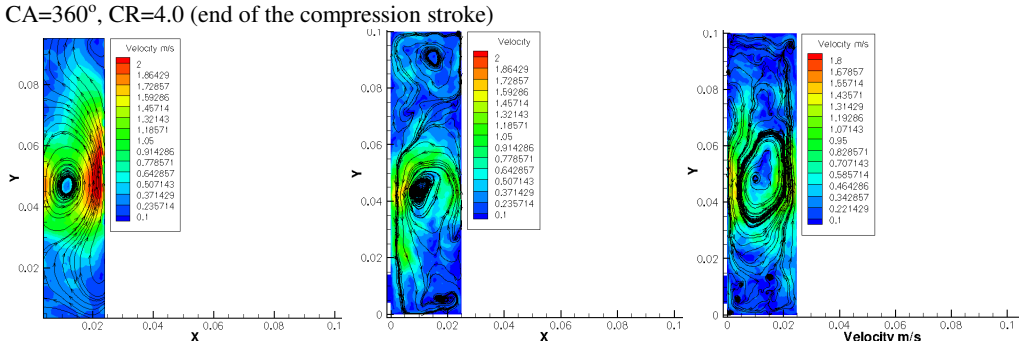

Experiment Present LES Present PANS

Figure 5: Temporal/spatial evolution of the phase-averaged velocity field. The contours are coloured by the velocity magnitude

CA=29.9°, CR=3.3 (intake stroke)

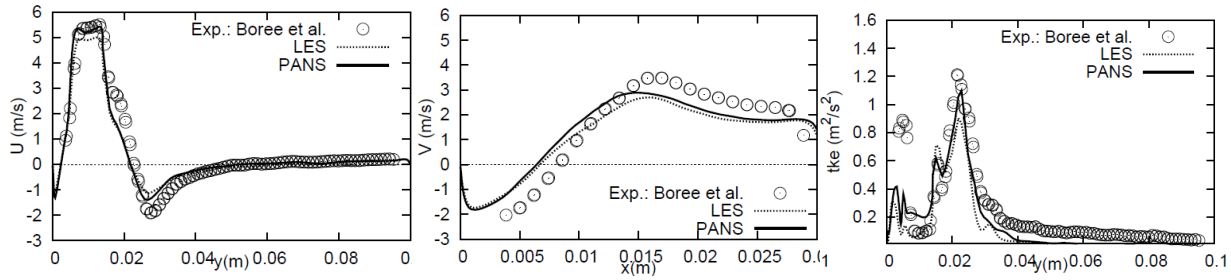

CA=86.2°, CR=1.67 (intake stroke)

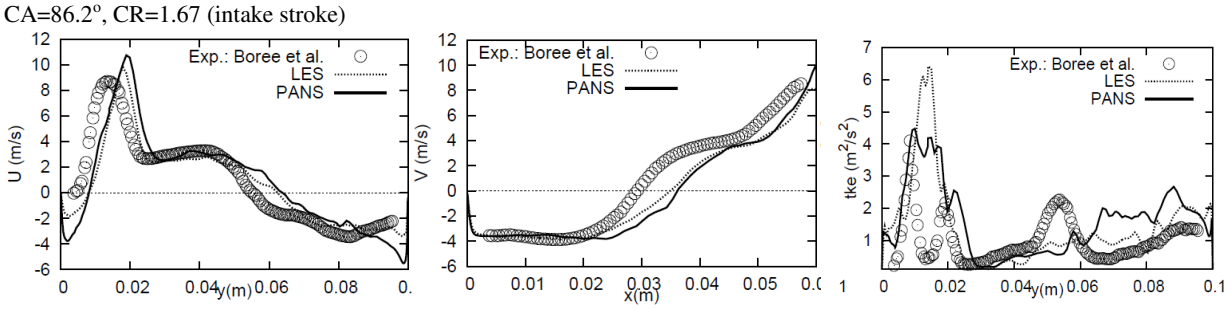

CA=180°, CR=1.0 (end of the intake stroke)

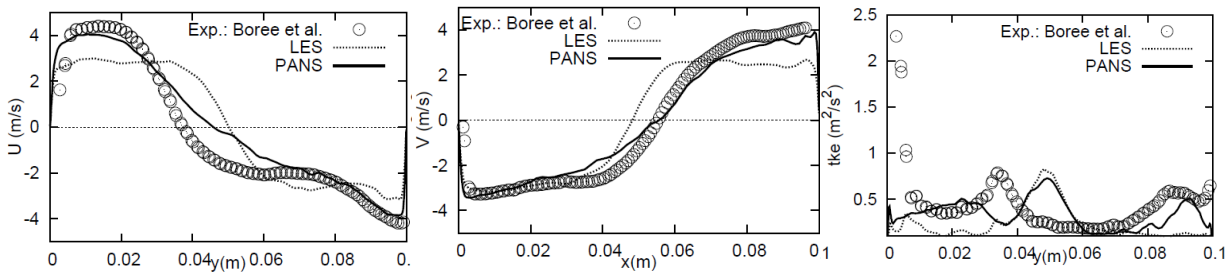

CA=273.8°, CR=1.67 (compression stroke)

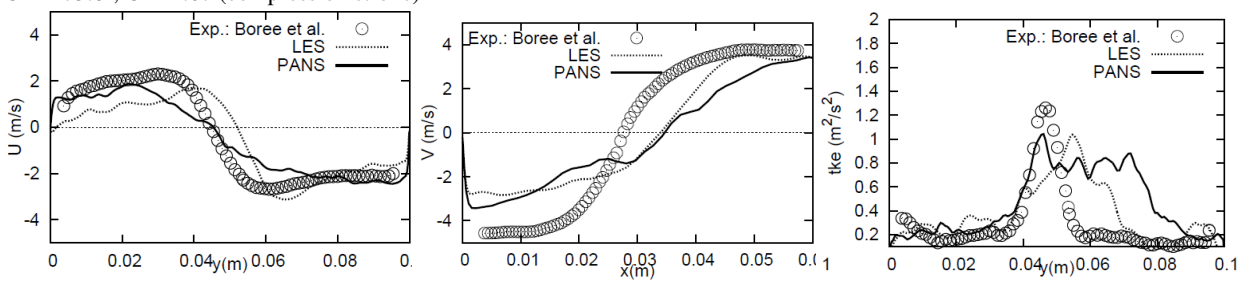

CA=360°, CR=4.0 (end of the compression stroke)

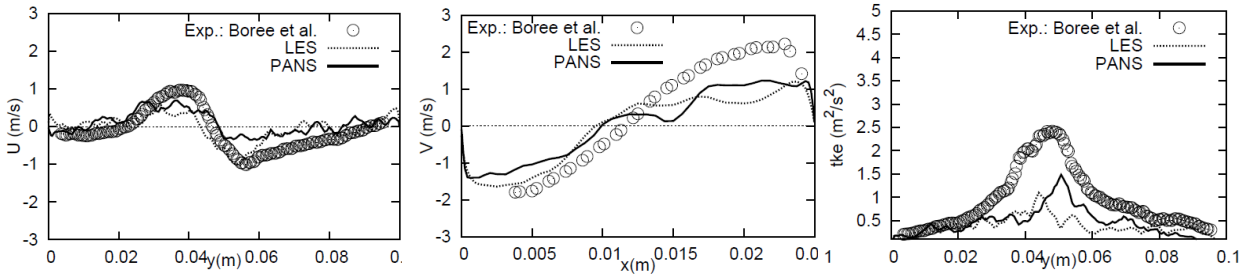

Figure 6: Evolution of the phase-averaged mean velocity and turbulent kinetic energy profiles in the central vertical plane